Available online at www.sciencedirect.com
SCIENCE DIRECT®
Journal of Solid State Chemistry 178 (2005) 655–660
JOURNAL OF SOLID STATE CHEMISTRY
www.elsevier.com/locate/jssc

'Soft' phonon modes, structured diffuse scattering and the crystal chemistry of Fe-bearing sphalerites

Ray L. Withers[a,*], T.R. Welberry[a], Allan Pring[b], Cristophe Tenailleau[b], Yun Liu[a]

[a]*Research School of Chemistry, Australian National University, Canberra, ACT, 0200, Australia*
[b]*Mineralogy Department, South Australian Museum, Adelaide, South Australia*

Received 19 October 2004; received in revised form 9 December 2004; accepted 10 December 2004

Abstract

Electron diffraction has been used to carefully investigate the reciprocal lattices of a range of iron-bearing sphalerites looking for evidence of Fe clustering and/or Fe/Zn ordering in the form of either additional satellite reflections or a structured diffuse intensity distribution accompanying the strong Bragg reflections of the underlying sphalerite-type average structure. While a highly structured diffuse intensity distribution in the form of transverse polarized $\{110\}^*$ sheets of diffuse intensity has been detected and found to be characteristic of all compositions, it does not appear to arise from Fe clustering and/or Fe/Zn ordering. Rather inherently low frequency, and therefore strongly thermally excited, phonon modes propagating along reciprocal space directions perpendicular to each of the six $\langle 110 \rangle$ real space directions of the average structure are suggested to be responsible for these $\{110\}^*$ sheets of diffuse intensity. Monte Carlo simulation (for a range of Zn–S, Zn–Zn and S–S interaction strengths) and subsequent Fourier transformation is used to confirm the existence of these low-frequency phonon modes of distortion as well as to show that they are an intrinsic, predictable property of the corner-connected tetrahedral structure of sphalerite. The low-frequency phonon modes involve coupled (Zn, Fe) and S motion in one-dimensional strings along $\langle 110 \rangle$ real space directions.

Keywords: Soft phonon modes; Structured diffuse scattering; Fe-bearing sphalerites

1. Introduction

The high symmetry $F\bar{4}3m$ sphalerite, ZnS, structure type is well-known and can be described in terms of ZnS_4 (or equally validly SZn_4) tetrahedra each corner connected to four neighboring such tetrahedra in the manner shown in Fig. 1a. The extent as well as the mechanism underlying Fe substitution into sphalerite, ZnS, is of interest both from the fundamental point of view of substitutional sphalerite equilibria as well as for the understanding of the kinetics of mineral formation of sphalerite-bearing paragenesis [1–5]. The maximum solubility of FeS in ZnS has recently been shown to depend strongly upon sulfur fugacity with an upper solubility limit (at 700 °C) ranging from 21 mol% for a low sulfur fugacity $Fe_{1-x}S/FeS_2$ buffer up to as high as 52 mol% for a high sulfur fugacity Fe/FeS buffer [1]. The valence state, or states, in which Fe substitutes into the sphalerite average structure type, and hence the extent of local substitutional strain, has also been reported to be strongly dependent upon sulfur fugacities [1]. Higher sulfur fugacities have been correlated with increased Fe^{3+} (and associated metal vacancy) concentrations at fixed Zn/Fe ratios. Likewise noticeable differences in reported lattice parameter behavior as a function of Fe content above ~10 mol% have also been correlated with variable sulfur fugacities.

Mössbauer spectra of Fe-containing sphalerites are known to change from a singlet to a doublet for Fe contents >~6 mol% [6,7]. This has been attributed to the onset of Fe–Fe bonding interactions and local Fe

*Corresponding author. Fax: +61 2 6125 0750.
E-mail address: withers@rsc.anu.edu.au (R.L. Withers).

0022-4596/$ - see front matter © 2004 Elsevier Inc. All rights reserved.
doi:10.1016/j.jssc.2004.12.011

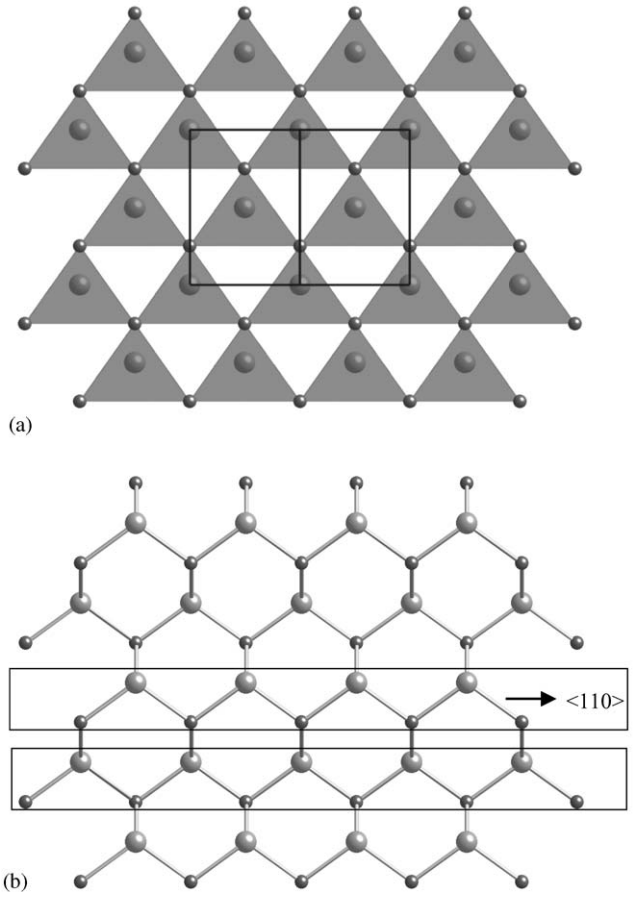

Fig. 1. The ideal $F\bar{4}3m$ ZnS tetrahedral, corner-connected ideal sphalerite structure type is shown in projection down a $\langle 110 \rangle$ direction in: (a) polyhedral mode and (b) ball and stick mode. The Zn ions are represented by the large gray balls and the S ions by the smaller darker balls. The ZnS_4 tetrahedra are shaded in (a).

clustering above a critical Fe content in ZnS and has lead to speculation about possible "… ordering phenomena depending on the Fe content …" in Fe-bearing sphalerites [1]. Balabin and Sack [8] have similarly predicted that Fe-bearing sphalerites have a tendency to "… undergo long range ordering to lower symmetry structures …" and have underscored a "… need for better characterization of the structures of (Zn,Fe)S minerals…". Ordering phenomena of this type have the potential to give rise either to structured diffuse scattering and/or additional satellite reflections accompanying the strong Bragg reflections of the underlying sphalerite-type average structure. In the crystal chemically not unrelated-$Fe_{1-x}O$ wüstite solid solution, e.g., Fe^{2+}/Fe^{3+} ordering and associated structural relaxation has long been known to give rise to a highly structured and characteristic diffuse intensity distribution [9]. The purpose of the current paper is to report the results of a search for any such additional structured diffuse scattering and/or satellite reflections in a range of Fe-bearing sphalerites.

2. Experimental

2.1. Samples

Fe-containing sphalerites from a range of locations and geological conditions (see Table 1) were selected for examination. All samples lie close to the ZnS–FeS joint. Chemical analyses were undertaken using a Cameca CAMEBAX SX51 electron microprobe at Adelaide Microscopy, University of Adelaide. The analyses were undertaken using an accelerating potential of 20 kV and a specimen current of ~20 nA. The spot size was set at 1 μm but the effective resolution of the beam due to beam spread in the sample was of the order of 3 μm. The following standards were used for wavelength dispersive analysis: natural pentlandite (Ni, Fe), natural sphalerite (Zn,S), natural cobaltite (Co), natural rhodonite (Mn), natural chalcopyrite (Cu) and Cd metal (Cd).

2.2. X-ray powder diffraction

The cubic average structure unit cell dimensions of the various samples were determined via X-ray diffraction using a using a Guinier-Hägg XRD camera with Cu $K_{\alpha 1}$ radiation. Silicon (NBS No.640) was added as an internal standard for accurate determination of the unit cell dimensions, which were refined using the Unitcell software package [10].

2.3. Electron diffraction

Crushed specimens were deposited on holey-carbon coated grids and examined in a Philips EM 430 Transmission Electron Microscope operating at 300 kV.

3. Results

3.1. EPMA results

The Fe contents of the selected samples were carefully examined by electron probe microanalysis (EPMA) for homogeneity and chemical composition using the analytical conditions described above. Insignificant amounts of Cd, Mn and Cu were detected in the Fe-bearing sphalerite grains so that the specimens lie very close to the ZnS–FeS joint. The Fe content of these grains was determined by EPMA to range effectively from zero up to a maximum of 0.174 (see Table 1).

3.2. X-ray powder diffraction

The refined cubic unit cell dimensions are given in Table 1. They are in reasonably good agreement with those reported in the literature [1]. Typical XRD patterns (of the G25134 and G25646 samples, 0.1 and

Table 1
EPMA analyses of the various Fe-bearing sphalerite mineral samples investigated

Specimen	Location	Cd	Mn	Fe	Zn	Cu	S	Total	Cell (Å)	mol%Fe
G25134	Picos do Uropa, Spain	0.10	0.01	0.05	65.66	0.03	33.63	99.48	5.408(1)	0.1
G11281	Wallaroo Mines, South Australia	0.24	0.0	1.79	63.64	0.0	34.33	100.00	5.410(1)	3
G12654	Durham, U.K	0.24	0.00	2.99	62.28	0.06	32.80	98.36	5.411(1)	5.3
G13817	Taylor Farm, Madoc, Canada	0.36	0.01	3.68	62.61	0.01	32.83	99.50	5.411(1)	6.5
G25646	Broken Hill, NSW	0.17	0.09	9.74	55.61	0.03	32.80	98.44	5.418(1)	17.4

The element content is given in wt%.

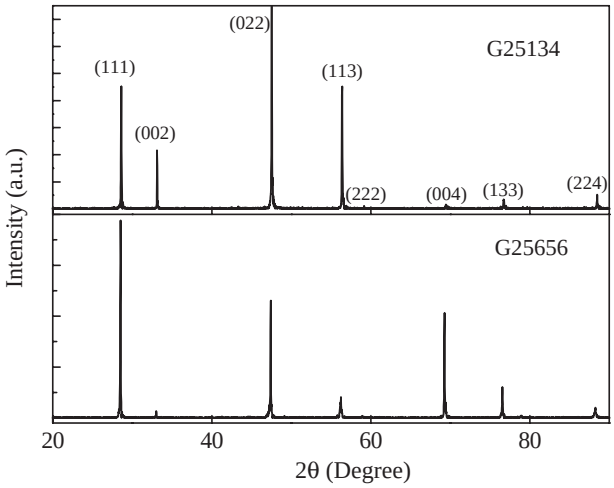

Fig. 2. XRD patterns of the G25134 and G25646 samples (0.1 and 17.4 mol% Fe, respectively).

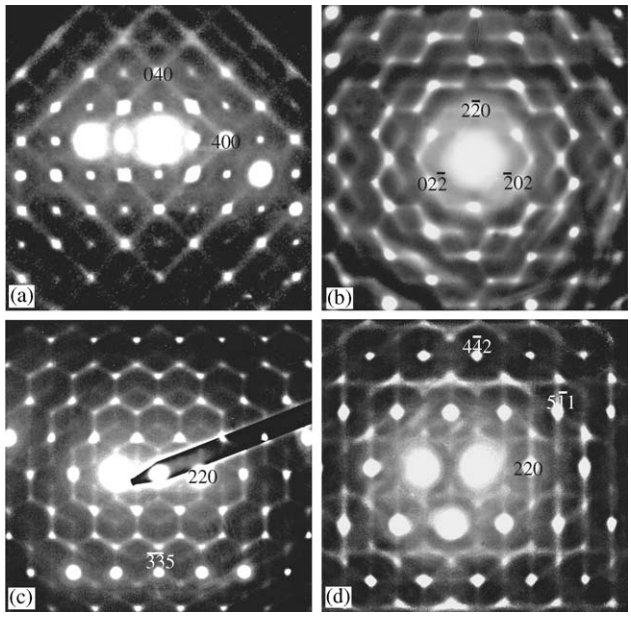

Fig. 3. (a) close to ⟨001⟩, (b) close to ⟨111⟩, (c) ~[556] and (d) ⟨114⟩ zone axis electron diffraction patterns (EDP's) typical of each of the various Fe-bearing sphalerite samples. (a) and (c) are from the maximum Fe content (G25646) sample while (b) and (d) are from the 5.3 mol% (G12654) sample. Indexation is with respect to the underlying sphalerite-type average structure.

17.4 mol% Fe, respectively) obtained using a Siemens (D5000) powder diffractometer are shown in Fig. 2.

3.3. Electron diffraction

Fig. 3 shows (a) close to ⟨001⟩, (b) close to ⟨111⟩, (c) ~[556] and (d) ⟨114⟩ zone axis electron diffraction patterns (EDP's) typical of each of the various Fe-bearing sphalerite samples. Figs. 3a and c are from the maximum Fe content (G25646) sample while Figs. 3b and d are from the 5.3 mol% (G12654) sample. Note the presence of a highly structured and extremely characteristic diffuse intensity distribution present in one form or another at all zone axis orientations. To zeroth order, this takes the form of transverse polarized, {110}* sheets of diffuse intensity perpendicular to each of the six ⟨110⟩ directions of the $F\bar{4}3m$ underlying average structure. At any one zone axis orientation, this gives rise to transverse polarized diffuse streaking along excited ⟨*hhl*⟩* directions of reciprocal space perpendicular to any of the six ⟨110⟩ real space directions, e.g., along the ⟨511⟩*, ⟨442⟩* and ⟨220⟩* directions in Fig. 3d, the ⟨224⟩* directions in Fig. 3b, etc. The transverse polarized character of this observed diffuse distribution, i.e., the fact that the intensity of the observed ⟨*hhl*⟩* streaking is always strongest when looking out along directions of reciprocal space perpendicular to the direction of the streaking itself (particularly apparent in Fig. 3a), requires that it must be generated primarily by displacements of the constituent metal ($Zn_{1-x}Fe_x$) and S ions along the ⟨110⟩ directions perpendicular to each of the {110}* diffuse sheets (see Fig. 1b).

Close to ⟨001⟩ zone axis orientations (see e.g., Fig. 3a and Fig. 4), these {110}* diffuse sheets take the form of essentially continuous diffuse streaking along the ⟨110⟩* and ⟨1$\bar{1}$0⟩* directions of reciprocal space running primarily (i.e., with the strongest intensity) through the $h+k=4J$ (J an integer) average structure Bragg reflections. On tilting away from ⟨001⟩ towards a ⟨111⟩ orientation, however, the ⟨*hhl*⟩* diffuse streaking becomes more and more segmented (see, e.g., the quite segmented ⟨511⟩*-type

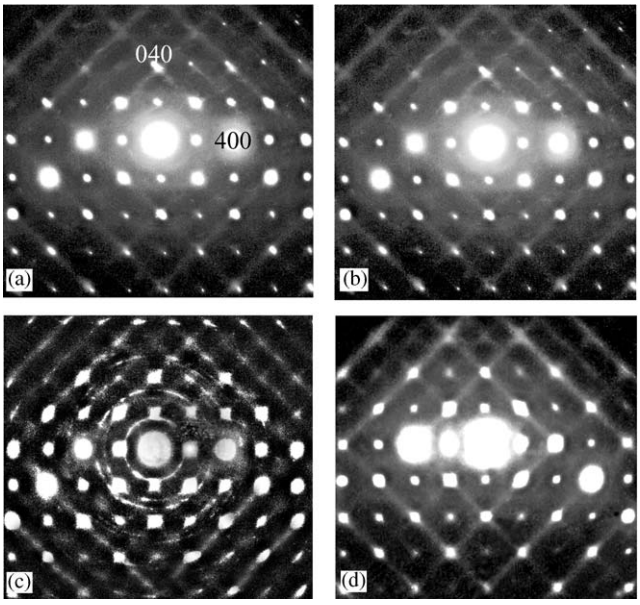

Fig. 4. Close to ⟨001⟩ zone axis electron diffraction patterns (EDP's) of the (a) G25134, (b) G11281, (c) G13817 and (d) G25646 samples.

diffuse streaking in Fig. 3d) until a rather beautiful honeycomb pattern of structured diffuse intensity is observed in the vicinity of the ⟨111⟩ zone axis orientation (see e.g. Figs. 3b and c). This sharp variation in relative intensity of the $\langle hhl\rangle^*$ diffuse streaking with orientation and position in reciprocal space cannot be attributed to the rather more slowly varying effect associated with the displacement shift direction of the metal and S ions but rather arises from an interference effect between the contributions of the metal and S ion sub-lattices to the structure factor of the relevant diffuse sheet as is illustrated below.

No direct diffraction evidence could be found for the dependence of the observed diffuse distribution upon Fe content (see e.g., the close to ⟨001⟩ zone axis EDP's of the 0.1, 3, 6.5 and 17.4 mol% Fe samples shown in Fig. 4) suggesting that it arises primarily from the thermal excitation of specific low-frequency phonon modes of distortion of the ideal corner-connected tetrahedral structure of sphalerite (see Fig. 1) and is not strongly affected by Fe/Zn substitution. Nor was there any additional diffuse intensity that could be attributed to the effects of Fe/Zn substitution, suggesting that Fe substitutes overwhelmingly in the 2+form (for the specimens we have investigated) thereby minimizing local substitutional strain. Bond valence sum considerations [11], e.g., suggest that the ideal metal (M)–S bond length need undergo only a very slight expansion from 2.347 Å for $M = Zn^{2+}$ to 2.417 Å for $M = Fe^{2+}$. Substitution of Fe in the 3+form, however, would necessitate the introduction of metal ion vacancies and could be expected to have a much larger effect upon the observed diffuse distribution.

4. Interpretation

Transverse polarized, $\{110\}^*$ sheets of diffuse intensity in reciprocal space (see Fig. 3) imply the existence of ⟨110⟩ columns of atoms in real space whose displacements (along the same ⟨110⟩ direction) are correlated within a column but uncorrelated from one such column to the next as schematically illustrated in Fig. 1b (where two such neighboring ⟨110⟩ columns are shown contained in rectangular boxes). A similar pattern of correlated atomic displacements in ⟨110⟩ columns was first proposed many years ago by Honjo et al. [12] to explain the presence of a very similar pattern of structured diffuse intensity observed in the closely related cases of Si and Ge.

Given that the strongest restoring force constants in the case of sphalerite can be expected to be associated with the nearest neighbor metal-S bonds (represented by the sticks in Fig. 1b), it is easy to see why such a correlated pattern of atomic displacements might have a quite low frequency and hence be strongly thermally excited, to first order, and provided the displacement of the metal ions along ⟨110⟩ have the same magnitude as that of the S ions (so that all of the ions contained within any one rectangular box in Fig. 1b shift the same amount along ⟨110⟩), such atomic displacements do not, to first order, alter any of the local metal-sulfur bond lengths and hence would be subject to a very weak restoring force if only Zn–S interactions were taken into account. It is also easy to see why such columnar correlated atomic displacements do not need to be correlated from one such column to the next in the orthogonal $\langle h\bar{h}l\rangle^*$ directions and hence give rise to the observed transverse polarized, $\{110\}^*$ sheets of diffuse intensity. The observed diffuse distribution in this sense maps out the intrinsic low-frequency modes of distortion of the ideal sphalerite structure type.

It is not so easy, however, to see why the proposed columnar displacements give rise to the observed honeycomb-type diffuse distribution in the vicinity of ⟨111⟩ orientations (see Figs. 3b and c) or what can be learnt about the forces operating in such systems from the observed diffuse distribution. For this, we turn to Monte Carlo simulation.

4.1. Monte Carlo simulation

Monte Carlo (MC) simulations of real space distributions were therefore carried out using an array of $48 \times 48 \times 48$ real space unit cells and periodic boundary conditions. We ignore the presence of substituting Fe ions for the purposes of the simulation and include simple Hooke's law (harmonic) springs to represent nearest neighbor Zn–S, Zn–Zn and S–S interactions. Spring force constants for Zn–S:Zn–Zn:S–S were assigned relative values in the ratios (a) 40:1:1, (b)

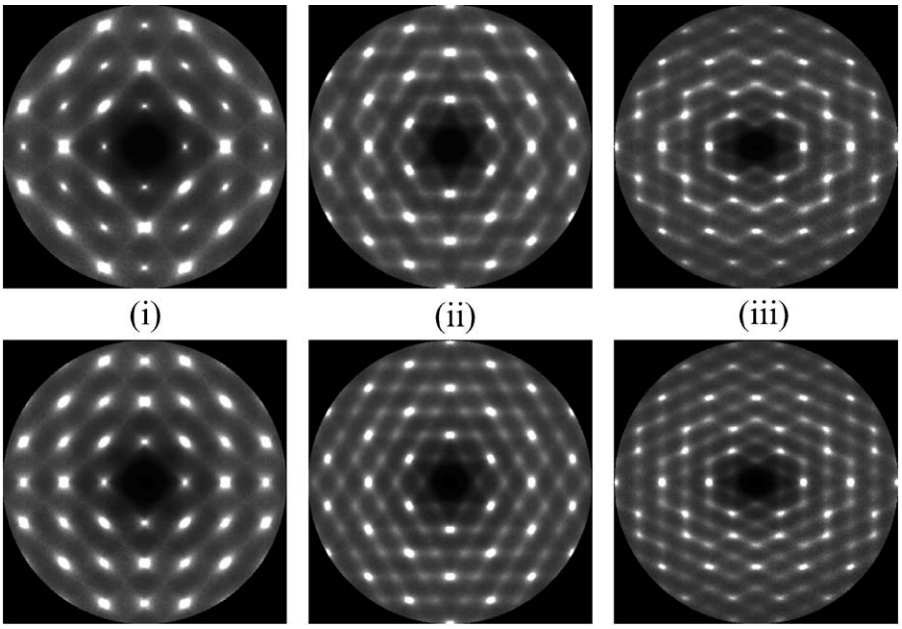

Fig. 5. Simulated (i) ⟨001⟩, (ii) ⟨111⟩ and (iii) ⟨556⟩ EDP's for the 2:1:1 and 1:8:8 force constant ratios for comparison with the experimental EDP's shown in Figs. 3a–c.

2:1:1 and (c) 1:8:8. During iteration the magnitudes of the force constants were adjusted relative to the simulation temperature $kT = 1$, though their relative values were maintained. This adjustment was made after lattice averages had been computed at the end of each cycle of iteration and was made in order to maintain a constant value for B_{iso} of 1.0 Å^2 for all atoms. Iteration was carried out for 800 MC cycles, where a cycle is defined as that number of individual MC steps required to visit each atom once on average.

Diffraction patterns of various reciprocal space sections were calculated from the final distribution using the program DIFFUSE [13] and these may be compared directly with the experimentally observed EDP's. Fig. 5 shows simulated (i) ⟨001⟩, (ii) ⟨111⟩ and (iii) ⟨556⟩ EDP's for the 2:1:1 and 1:8:8 force constant ratios for comparison with the experimental EDP's shown in Figs. 3a–c. The simulated EDP's for the 40:1:1 case are rather similar to those shown for the 2:1:1 case.

In qualitative terms, the agreement is remarkably good for both the 2:1:1 and 1:8:8 cases—particularly if allowance is made for some (unavoidable) redistribution of the simulated diffuse intensity arising from the effects of multiple scattering involving the strong average structure Bragg reflections (cf., e.g., Fig. 5c with Fig. 3c). This confirms that the proposed correlated (within the column but not from column to column) rod-like motion of the ions within the rectangular boxes of Fig. 1b is indeed responsible for the observed diffuse distribution. There are, however, subtle differences in the simulated EDP's between the 2:1:1 and 1:8:8 cases,

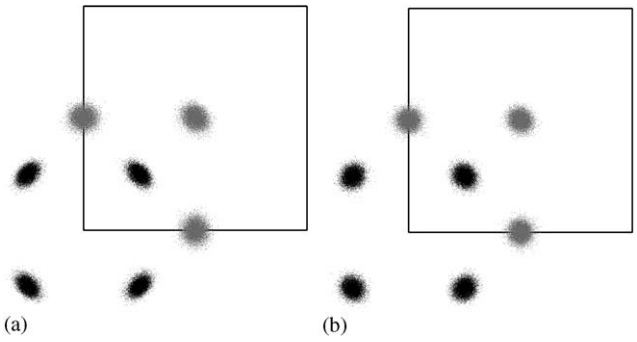

Fig. 6. Positionings (in each of the $48 \times 48 \times 48$ unit cells simulated cells) of the nearest neighbor S (black) and Zn (gray) ions relative to a central Zn ion for: (a) the 40:1:1 and (b) the 2:1:1 cases in projection along an ⟨001⟩ direction.

e.g., the relative intensity of the simulated $h + k = 4J + 2$ to the $h + k = 4J$ reflections (cf. Fig. 5a–d) is clearly strongly affected by the relative strengths of the Zn–S to Zn–Zn and S–S interactions. The experimental close to ⟨001⟩ zone axis EDP suggests that the former 2:1:1 ratio is rather closer to the mark than the 1:8:8 ratio. Likewise, the segmentation of the $\langle\bar{2}\bar{2}4\rangle^*$-type diffuse streaking responsible for the observed honeycomb-type diffuse distribution in the vicinity of ⟨111⟩ orientations (see e.g. Figs. 3b and c) appears rather better simulated by the 2:1:1 (or higher) ratio rather than the 1:8:8 ratio.

While the (presumably) thermally excited ⟨110⟩ shifts within individual ⟨110⟩ columns (see Fig. 1b) are clearly highly anisotropic, the fact that there exist six

such ⟨110⟩ columns along which ⟨110⟩ displacements are simultaneously taking place means that the resultant displacements of individual ions end up being isotropic. Likewise, the relative positioning of any one Zn or S ion to its nearest neighbor Zn and S ions is also relatively isotropic. Fig. 6, e.g., shows the positioning (in each of the $48 \times 48 \times 48$ unit cells simulated cells) of the nearest neighbor S (black) and Zn (gray) ions relative to a central Zn ion for (a) the 40:1:1 and (b) the 2:1:1 cases in projection along a ⟨001⟩ direction. Only in the former 40:1:1 case do the S ions vibrate markedly anisotropically and perpendicular to the local Zn–S bond.

4.2. Crystal chemical considerations

Assuming that Fe can substitute for Zn^{2+} in either the Fe^{2+} or Fe^{3+} form and that the S array remains fully occupied after such substitution/s, the resultant stoichiometry can be written as

$$(Zn^{2+})_{(1-x-2y)/(1+y)}(Fe^{2+})_{x/(1+y)}(Fe^{3+})_{2y/(1+y)}\square_{y/(1+y)}S$$

The suggested introduction of Fe in the 3+form [1] thus necessitates the introduction of vacancies at the $y/(1+y)$ level on the metal ion sites which one would expect to have a strong effect upon the correlation length of the observed phonon modes. No evidence for any such effect was observed experimentally suggesting that the overwhelming majority of the substituted Fe is in the 2+form. From the bond valence sum point of view this would be distinctly advantageous in that the ideal metal (M)–S bond length is 2.3465 Å for $M = Zn^{2+}$ and 2.4165 Å for $M = Fe^{2+}$ [10]. Such a substitution could be expected to have minimal effect in terms of substitutional strain apart from a slight increase in cell parameter with increasing Fe^{2+} content.

5. Conclusions

A highly structured diffuse intensity distribution in the form of transverse polarized {110}* sheets of diffuse intensity has been found to be characteristic of a range of Fe-bearing sphalerite mineral samples. Inherently low-frequency phonon modes propagating along reciprocal space directions perpendicular to each of the six ⟨110⟩ real space directions of the average structure are suggested to be responsible for these {110}* sheets of diffuse intensity. No diffraction evidence could be found for Fe clustering and/or Fe/Zn ordering in any of the Fe-bearing sphalerite mineral samples.

References

[1] P. Lepetit, K. Bente, T. Doering, S. Luckhaus, Phys. Chem. Minerals 30 (2003) 185–191.
[2] K. Bente, Th. Doering, Eur. J. Mineral. 5 (1993) 465–478.
[3] K. Bente, Th. Doering, Mineral. Petrol. 53 (1995) 285–305.
[4] P.B. Barton, P. Toulmin III, Econ. Geol. 61 (1966) 815–849.
[5] P.B. Barton, P.M. Bethke, Am. Mineral. 72 (1987) 451–467.
[6] J.D. Keys, J.L. Horwood, T.M. Baleshta, L.J. Cabri, D.C. Harris, Can. Mineral. 9 (1968) 453–467.
[7] A. Gerard, P. Imbert, H. Prange, F. Varret, M. Winterberger, J. Phys. Chem. Solids 32 (1971) 2091–2100.
[8] A.I. Balabin, R.O. Sack, Mineral. Mag. 64 (2000) 923–943.
[9] T.R. Welberry, A.G. Christy, Phys. Chem. Minerals 24 (1997) 24–38.
[10] B. Noläng, Inst. Materialkemi, Ångströmlaboratoriet, Box 538, SE-751 21, Uppsala, Sweden.
[11] N.E. Brese, M. O'Keeffe, Acta Crystallogr. B 47 (1991) 192–197.
[12] G. Honjo, S. Kodera, N. Kitamura, J. Phys. Soc. Japan 19 (1964) 351–367.
[13] B.D. Butler, T.R. Welberry, J. Appl. Cryst. 25 (1992) 391–399.